
Article:
Ai, S., Lu, B., Chen, J. et al. (2 more authors) (2017) Evaluation of deformation stability and fracture mechanism in incremental sheet forming. International Journal of Mechanical Sciences, 124-125. pp. 174-184. ISSN 0020-7403

https://doi.org/10.1016/j.ijmecsci.2017.03.012

Evaluation of deformation stability and fracture mechanism in incremental sheet forming

S. Ai, B. Lu, J. Chen, H. Long, H. Ou

www.elsevier.com/locate/ijmecsci

PII: S0020-7403(16)31065-7
DOI: http://dx.doi.org/10.1016/j.ijmecsci.2017.03.012
Reference: MS3624

To appear in: *International Journal of Mechanical Sciences*

Received date: 12 December 2016
Revised date: 7 March 2017
Accepted date: 8 March 2017

Cite this article as: S. Ai, B. Lu, J. Chen, H. Long and H. Ou, Evaluation o deformation stability and fracture mechanism in incremental sheet forming *International Journal of Mechanical Sciences* http://dx.doi.org/10.1016/j.ijmecsci.2017.03.012

Evaluation of deformation stability and fracture mechanism in incremental sheet forming

S. Ai[a, b], B. Lu[a, b*], J. Chen[a], H. Long[b], H. Ou[c]

[a] Department of Plasticity Technology, Shanghai Jiao Tong Univesity, 1954 Huashan Rd, Shanghai, 200030, China

[b] Department of Mechanical Engineering, University of Sheffield, Sheffield, S1 3JD, UK

[c] Department of Mechanical, Materials and Manufacturing Engineering, University of Nottingham, Nottingham, NG7 2RD, UK

[*]Corresponding author. Tel.: +86 21 62813430. E-mail address: binlu@sjtu.edu.cn

Abstract:

Incremental sheet forming (ISF) is a flexible process for rapid manufacturing of complex sheet metal parts. An advantage of ISF is the improved formability than traditional sheet forming processes such as stamping. A number of fundamental studies have been conducted to investigate the enhanced ISF formability considering the effects such as bending under tension and through thickness shear. To further understand the ISF deformation mechanism and formability enhancement, this work presents a new analytical model which is focused on investigating the deformation stability and its effect on the metal sheet fracture. Based on this new model, the critical strain of deformation instability is obtained. Furthermore, influences of the work-hardening effect and bending effect on the deformation stability are investigated. To validate the analytical model, the fracture occurrence of two aluminum grades, AA1100 and AA5052, are investigated by using ISF experiment. Based on the analytical and experimental investigation, this study has concluded that bending plays a major role on ISF deformation stability. In addition, the ISF fracture depends on both deformation stability and the sheet material's ductility.

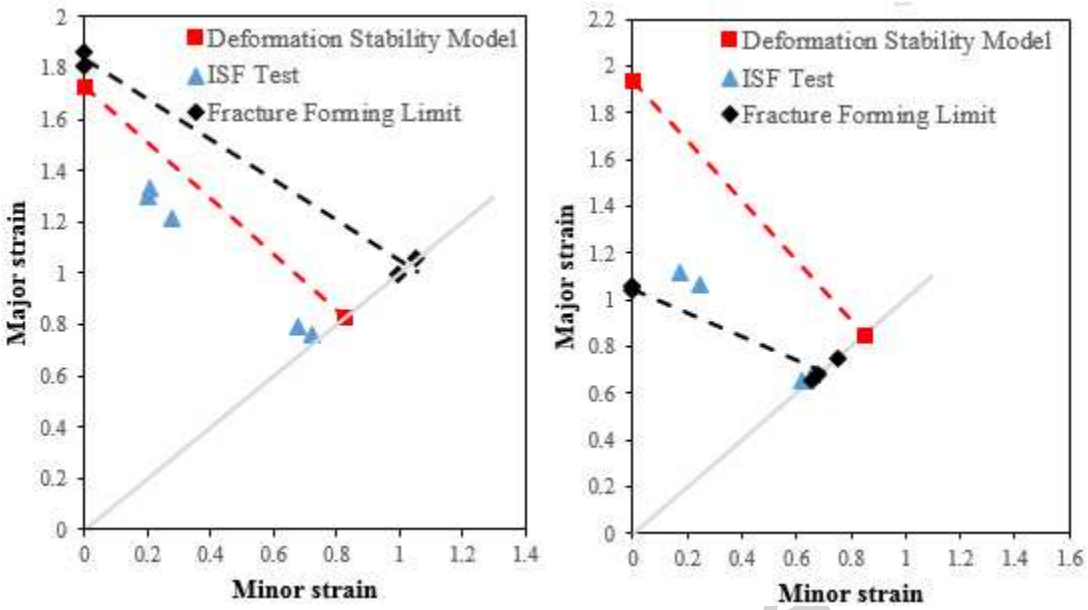

(a) (b)

Fig.1 Comparison of formability: (a) AA1100; (b) AA5052

Key words: incremental sheet forming, deformation instability, formability, fracture

*

Nomenclature

σ_{φ}^{X}	Meridional stress in region X (MPa)
σ_{θ}^{X}	Circumferential stress in region X (MPa)
σ_{t}^{X}	Thickness stress in region X (MPa)
σ_{s}^{X}	Yield stress in region X (MPa)
F_{φ}^{X}	Force in meridional direction on region X (N)
F_{t}^{X}	Force in thickness direction on region X (N)
F_{θ}^{X}	Force in tangential direction on region X (N)
$\varepsilon_{\varphi}^{X}$	Meridional strain in region X
ε_{θ}^{X}	Circumferential strain in region X
ε_{t}^{X}	Thickness strain in region X
α	Forming angle (radian)
θ_0	Circumferential contact angle (radian)
β	Meridional contact angle (radian)
r_t	Tool radius (mm)
r	Distance to tool center (mm)
t_0	Initial sheet thickness (mm)
t	Actual sheet thickness (mm)
S	Transition area between region A and B (mm^2)
$\bar{\varepsilon}$	Equivalent strain

1. Introduction

Incremental sheet forming (ISF) is a flexible process for manufacturing small-batch and customized sheet metal products. Compared with conventional sheet forming technologies, no delicate forming tools are required in the ISF process, the rigid tool moves along a predefined toolpath and the sheet metal deforms incrementally in the localized contact area. As ISF does not require specified tool set or dedicated forming press, cost and production-lead time can be reduced considerably. In recent years, tremendous efforts have been made to further improve this technology. Apart from the conventional single point incremental sheet forming (SPIF), other technologies such as two point incremental forming (TPIF) [1] and double side incremental forming process (DSIF) [2] have been proposed. To further expand the ISF potential, hot ISF technologies such as laser assisted incremental forming [3] and electric assisted incremental forming [4] have also been developed recently.

In order to obtain an in-depth understanding of the ISF deformation behavior, process and material related parameters were investigated experimentally and analytically. Silva et al. [5] developed an analytical model to investigate the influence of friction and other process parameters on the formability. Martins et al. [6] adopted membrane analysis method to analyze and compare the formability in plane-strain condition and equibiaxial tension condition. Xu et al. [7] investigated the influence of tool rotation on ISF process with a rotational textured tool. Fratini et al. [8] employed a statistical method to analyze the influence of material-related parameters like work-hardening exponent and compared their degree of importance. Kim et al. [10] verified the effects of tool size, feed rate and friction on formability, and found that the effect of friction was insignificant. Fang et al. [11] confirmed the effect of bending deformation and analyzed the fracture behavior in ISF process. Lu et al. [12] investigated the effect of friction and fracture behavior with a novel oblique tool. He also proposed a new tool path generation algorithm to improve the capability of the process [9]. Huang et al. [13] analyzed the size effect in the SPIF process by using the Oyane fracture criterion.

A unique characterization of ISF process is its increased forming limit compared with conventional sheet forming processes. Shim et al. [14] and Park et al. [15] compared the ISF with conventional sheet forming process and found that the ISF forming limit was much higher. A lot of explanations on the deformation mechanism was proposed and analyzed. Young et al. [16] concluded that shear deformation of the sheet was the main cause of increased forming limit of ISF. Kim et al. [17] investigated the shear deformation by assuming the deformation is all shear in the thickness direction in the finite element analysis and found the thickness distribution matches with the experimental measurement. While Filice et al. [18]

concluded that stretching was the main deformation mode during the ISF process. Emmens et al. [19] conducted continuous bending under tension (CBT) test and considered bending as a major factor for the increase of forming limit. Jackson et al. [20] suggested that the deformation in ISF process was the combination of stretching, bending and shear. Allwood et al. [21] attributed the increased forming limit to the through-thickness shear, which reduced the accumulative breakage in the sheet material. Eyckens et al. [22] also analyzed the influence of through-thickness shear by using Marciniak-Kuczynski model. Malhotra et al. [23] discussed the effects of bending and shear on the stability of the process by using FE analysis. Emmens et al. [24] summarized the effects of the contact stress and cyclic loading on deformation localization, stability and increased formability during ISF process. Eyckens et al. [25] suggested that the dominant deformation mechanism depended on the specific process conditions. The above reported works focus on the effects of the increased ISF formability in a macro scale.

Although the above studies have partly clarified the improved formability and deformation stability by using experimental and FEM analysis, the understanding of the ISF deformation mechanism and the factors leading to sheet fracture is still limited. For example, plane strain state and equibiaxial stretching state are the most commonly seen when manufacturing parts of different geometrical shapes [14, 27]. However, only the deformation under plane strain state is well modelled while the equi-biaxial stretching state was usually ignored by the researchers. In addition, concerning the occurrence of fracture, a gradual necking may happen before fracturing for some materials, while for other materials this may not be the case [26]. The underlying mechanism of this behavior is still unclear.

To obtain an in-depth understanding of the fracture behavior and underlying mechanism, the presented work tries to develop an analytical model from the deformation stability point of view. In the model, to describe the ISF deformation stability, an analytical model has been established by taking both effects from sheet bending deformation and material strain hardening into account. The ISF deformation stability under both the plane-strain condition and equibiaxial stretching condition has been analyzed. The critical strain at which the forming sheet metal loses its deformation stability has been studied by using the developed model and been validated later by comparing ISF and bulge experiments using both AA1100 and AA5042 materials. The ISF deformation stability and the fracture mechanism have been discussed based on the analytical and experimental results.

2. Modeling of the deformation stability in the ISF process

In the conventional investigation of the ISF process, the influence of process and material mechanical parameters on the formability and fracture behaviour of the incremental forming process has already been widely explored, such as the effects form work-hardening exponent [8], the ratio between tool radius and sheet thickness [10] and bending [12]. In the conventional understanding of ISF, deformation could only occur in the tool-sheet contact area. Non-contact areas including the inclined wall are considered to be rigid or elastic. So, almost all analyses are based on the contact area. However, according to the recent experimental and FEM analysis, plastic deformation could also occur at the nearby inclined wall, where no tool-sheet contact exists [11]. A further research is needed to reassess the stability and fracture mechanism of ISF.

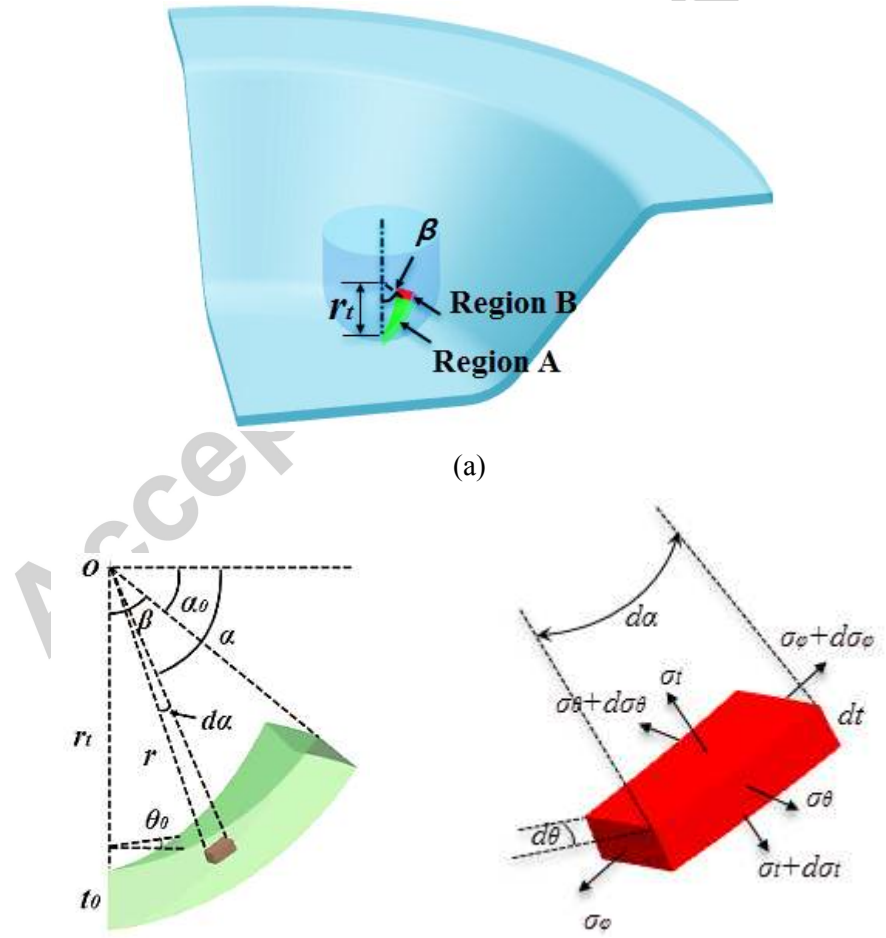

Fig. 1 Analytical modeling of ISF process: (a) Model definition; (b) Element definition in

region A; (c) Stress components of the element in region A

Focusing on the plastic deformation behavior in the contact and non-contact zone, an analytical model has been established as shown in Fig. 1. In this model, the tool-sheet contact region is defined as region A while the neighboring inclined wall is defined as region B. Due to the bending and stretching effect, region A is undergoing plastic deformation during the whole ISF process. However, the stress state of region B needs further investigation. In order to take bending into consideration, an element in the thickness direction of the sheet material in region A is taken for analysis, as shown in Fig. 1(c). The stress components of the element can be described as shown in Fig. 1(c). Concerning shear deformation, it has been found that comparing with bending and stretching, the effect from shear deformation can be neglected [12, 28]. Thus to simplify the analysis process, the friction and shear effect along the circumferential direction are ignored. Nevertheless, the impact of the tool movement still result in uneven stress distribution along the circumferential direction. At the same time, the force from the contact area will also lead to elastic deformation in the neighboring area, which may affect the boundary conditions for the analysis. However, in the present analytical method, ideal assumptions are made that the tool movement speed is considerably low and the vertical step is considerably small so that the impact of the tool movement can be largely reduced and the relatively small elastic deformation can be ignored. In addition, the material anisotropic effect is also ignored in this model.

2.1 Deformation Mechanics of Region A

During the ISF process, in the region A, there are two typical deformation modes: (1) plane-strain deformation when the circumferential contact angle is small and (2) equibiaxial stretching deformation when the circumferential contact angle is large, such as forming the corner area of a pyramid. In region B, the plane-strain condition is considered in all the case as the sheet does not directly contact with the forming tool and the sheet is subject to the tensile deformation in region A.

In region A, considering the effects of stretching and bending deformation, an equilibrium equation in the thickness direction may be established as:

$$\sigma_t^A \cdot r^2 \cdot d\alpha \cdot cos\alpha \cdot d\theta - \left(\sigma_t^A + d\sigma_t^A\right) \cdot \left(r + dr\right)^2 \cdot d\alpha \cdot cos\alpha \cdot d\theta$$
$$+\left(\sigma_\varphi^A + d\sigma_\varphi^A\right) \cdot dr \cdot \left(r + dr\right) \cdot cos\alpha \cdot d\theta \cdot sin\frac{d\alpha}{2} + \sigma_\varphi^A \cdot dr \cdot \left(r + dr\right) \cdot cos\left(\alpha + d\alpha\right) \cdot d\theta \cdot sin\frac{d\alpha}{2} \quad (1)$$
$$+\left(2\sigma_\theta^A + d\sigma\sigma_\theta^A\right) \cdot dr \cdot \frac{2r + dr}{2} \cdot d\alpha \cdot sin\frac{d\theta}{2} \cdot cos\alpha = 0$$

Eq. 1 can be simplified by neglecting the higher order terms:

$$\frac{d\sigma_t^A}{dr} = \frac{\sigma_\varphi^A + \sigma_\theta^A - 2\sigma_t^A}{r} \quad (2)$$

Considering the plane-strain condition $\sigma_\theta^A = \frac{1}{2}\left(\sigma_\varphi^A + \sigma_t^A\right)$ and equibiaxial stretching condition $\sigma_\theta^A = \sigma_\varphi^A$, the von Mises yield criterion $\sigma_s^A = \frac{1}{\sqrt{2}}\sqrt{\left(\sigma_\varphi^A - \sigma_\theta^A\right)^2 + \left(\sigma_\varphi^A - \sigma_t^A\right)^2 + \left(\sigma_\theta^A - \sigma_t^A\right)^2}$ is simplified by using a coefficient λ :

$$\sigma_s^A = \lambda\left(\sigma_\varphi^A - \sigma_t^A\right) \quad (3)$$

where under plane-strain condition, $\lambda = \frac{\sqrt{3}}{2}$ and under equibiaxial stretching condition, $\lambda = 1$.

Therefore, Eq.2 can be expressed as:

$$\frac{d\sigma_t^A}{dr} = 2\lambda\frac{\sigma_s^A}{r} \quad (4)$$

Considering the bending effect in the ISF process, as the sheet is bended around the tool in the meridional direction, the meridional strain can be expressed as:

$$\varepsilon_\varphi^A = \ln\frac{r}{r_t + \frac{t}{2}} + \ln\frac{t_0}{t} - \ln\frac{r_t}{r_t + \frac{t}{2}} = \ln\frac{r \cdot t_0}{r_t \cdot t} \quad (5)$$

Considering the strain hardening effect, the power hardening law $\sigma_s = K \cdot \bar{\varepsilon}^n$ is employed in this analysis. The relationship between the equivalent strain and strain components can be described by:

Plane-strain condition: $$\bar{\varepsilon} = \sqrt{\frac{2}{3}(\varepsilon_t^2 + \varepsilon_\theta^2 + \varepsilon_\varphi^2)} = \frac{2}{\sqrt{3}}\varepsilon_\varphi \quad (6)$$

Equibiaxial stretching condition: $$\bar{\varepsilon} = \sqrt{\frac{2}{3}(\varepsilon_t^2 + \varepsilon_\theta^2 + \varepsilon_\varphi^2)} = 2\varepsilon_\varphi \quad (7)$$

A new coefficient z may be introduced and a combined equation is obtained as:

$$\overline{\varepsilon} = z \cdot \varepsilon_{\varphi} \tag{8}$$

where under plane-strain condition, $z = \frac{2}{\sqrt{3}}$, and under equibiaxial stretching condition, $z = 2$.

Considering the power hardening law, Eq. 8 is obtained as:

$$\sigma_s^A = K \cdot \left(z \cdot \varepsilon_{\varphi}^A \right)^n \tag{9}$$

The stress in thickness direction in region A in Eq. 4 can be further derived as:

$$\sigma_t^A = 2\lambda \frac{K \cdot z^n}{n+1} \cdot \frac{t_0}{r_t \cdot t} \left\{ \left[\ln \frac{r \cdot t_0}{r_t \cdot t} \right]^{n+1} - \left[\ln \frac{(r_t + t) \cdot t_0}{r_t \cdot t} \right]^{n+1} \right\} \tag{10}$$

On the inner contact surface $r = r_t$, the contact stress can be described as:

$$\sigma_{tr}^A = 2\lambda \frac{K \cdot z^n}{n+1} \cdot \frac{t_0}{r_t \cdot t} \left\{ \left[\ln \frac{t_0}{t} \right]^{n+1} - \left[\ln \frac{(r_t + t) \cdot t_0}{r_t \cdot t} \right]^{n+1} \right\} \tag{11}$$

Considering the deformation area as a whole, the force equilibrium condition can be applied in the meridional, circumferential and thickness directions as shown in Fig. 2. It is noteworthy to mention here that the values of the stretching forces F_θ applied on the sides of the region A in the circumferential direction are assumed to be equal, as discussed in the beginning of this section. Meanwhile, the direction of F_θ and the contact force F_t can not be precisely determined due to the uneven distribution of the stress along both meridional and circumferential directions. However, according to Eq. (11), the contact stress increases along the depth direction while at the same time the contact area decreases. Force is the product of stress and area. As a result, it can be assumed that the overall force bearing point of the contact force F_t and the stretching force F_θ is right on the center of the contact surface and the boundary surface respectively, as shown in Fig. 2.

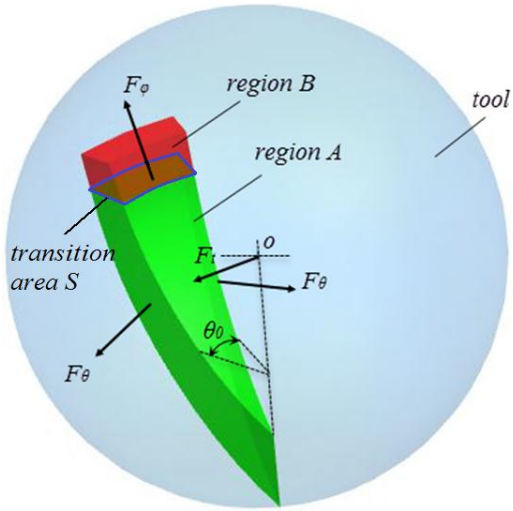

Fig. 2 Schematic illustration of the force components

In the meridional direction, the equilibrant equation can be given by,

$$F_\varphi^A = F_t^A \cdot \sin\frac{\beta}{2} + 2F_\theta^A \cdot \sin\frac{\theta_0}{2} \cdot \cos\beta \tag{12}$$

Similarly, force equilibrium equation in the circumferential direction can be expressed as:

$$F_t^A \cdot \cos\frac{\beta}{2} = 2F_\theta^A \cdot \sin\frac{\theta_0}{2} \cdot \sin\beta \tag{13}$$

Combining Eq.12 and Eq.13 together, it can be obtained that:

$$F_\varphi^A = F_t^A \cdot \left(\sin\frac{\beta}{2} + \frac{\cos\beta \cdot \cos\frac{\beta}{2}}{\sin\beta} \right) \tag{14}$$

The force component in the thickness direction F_t^A could also be considered as the integral of the contact stress in Eq. 11:

$$F_t^A = \int_{-\frac{\theta_0}{2}}^{\frac{\theta_0}{2}} \int_{\alpha_0}^{\frac{\pi}{2}} \left|\sigma_{tr}^A\right| \cdot r_t^2 \cdot d\alpha \cdot \cos\alpha \cdot d\theta \cdot \cos\theta \tag{15}$$

Considering the sheet thinning and strain, under plane-strain condition, the value of the sheet thinning can be expressed by using the Sine law

$$t = t_0 \cdot \cos\beta \tag{16}$$

In this way, the strain components can be calculated by:

$$\varepsilon_\varphi = -\varepsilon_t = -\ln\left(\cos\beta\right),\ \varepsilon_\theta = 0 \tag{17}$$

Similarly, under the equibiaxial stretching condition and with the volume conservation

assumption $\varepsilon_t + \varepsilon_\theta + \varepsilon_\varphi = 0$, the strain components can be obtained by:

$$\varepsilon_\varphi = \varepsilon_\theta = \ln\frac{l}{l_0} = -\ln(\cos\beta),\ \varepsilon_t = \ln\frac{t}{t_0} = -(\varepsilon_\theta + \varepsilon_\varphi) = 2\ln(\cos\beta) \tag{18}$$

and the sheet thickness under equibiaxial stretching condition can be obtained:

$$t = t_0 \cdot \cos^2\beta \tag{19}$$

By combining Eqs. 16 and 19, the relationship between sheet thickness and forming angle under plane-strain condition or equibiaxial stretching condition can be expressed in a combined model,

$$t = t_0 \cdot \cos^m\beta \tag{20}$$

where m is a coefficient, under plane-strain condition, $m = 1$, and under equibiaxial tensile state, $m = 2$.

Using Eq. 20, Eq. 17 can be solved as:

$$F_t^A = 2\lambda r_t^2 \frac{K\cdot z^n}{n+1}\theta_0 \cdot \int_{\alpha_0}^{\frac{\pi}{2}} \left\{ \left[\ln\frac{1}{\sin^m\alpha} \right]^{n+1} - \left[\ln\frac{(r_t + t_0\cdot\sin^m\alpha)}{r_t\cdot\sin^m\alpha} \right]^{n+1} \right\} \frac{\cos\alpha}{r_t\cdot\sin^m\alpha} d\alpha \tag{21}$$

Using Eq.24, the force component in the meridional direction can be obtained by:

$$\begin{aligned} F_\varphi^A = {} & 2\lambda r_t^2 \frac{K\cdot z^n}{n+1}\theta_0 \cdot \left(\sin\frac{\beta}{2} + \frac{\cos\beta\cdot\cos\frac{\beta}{2}}{\sin\beta} \right) \\ & \int_{\alpha_0}^{\frac{\pi}{2}} \left\{ \left[\ln\frac{1}{\sin^m\alpha} \right]^{n+1} - \left[\ln\frac{(r_t + t_0\cdot\sin^m\alpha)}{r_t\cdot\sin^m\alpha} \right]^{n+1} \right\} \frac{\cos\alpha}{r_t\cdot\sin^m\alpha} d\alpha \end{aligned} \tag{22}$$

2.2 Deformation Mechanics of Region B

Concerning region B, as there is no contact between the forming tool and the sheet metal, the normal contact stress is zero: $\sigma_t^B = 0$. In this region, plane-strain condition is considered as the sheet is under stretching in meridional direction. The von Mises stress is described as:

$$\sigma_s^B = \frac{1}{\sqrt{2}}\sqrt{(\sigma_\varphi^B - \sigma_\theta^B)^2 + (\sigma_\varphi^B - \sigma_t^B)^2 + (\sigma_\theta^B - \sigma_t^B)^2} = \frac{\sqrt{3}}{2}\cdot\sigma_\varphi^B \tag{23}$$

Combining the power hardening law and the equation (17), it can be obtained that:

$$\sigma_s^B = K\cdot\left(z\cdot\ln\frac{1}{\cos\beta} \right)^n \tag{24}$$

With Eq. 24, the meridional stress at region B can be obtained.

$$\sigma_{\varphi}^{B} = \frac{2}{\sqrt{3}} K \cdot \left(z \cdot \ln \frac{1}{\cos \beta} \right)^{n} \tag{25}$$

and the supporting force from region B can be given by:

$$F_{\varphi}^{B} = \sigma_{\varphi}^{B} \cdot S = \frac{2}{\sqrt{3}} K \cdot \left(z \cdot \ln \frac{1}{\cos \beta} \right)^{n} \cdot t_0 \cdot r_t \cdot \theta_0 \cdot \sin \beta \cdot \cos^{m} \beta \tag{26}$$

2.3 Deformation Instability in ISF

Concerning the deformation stability, in this model, the appearance of necking, which is caused by the yielding of the material in region B, is considered to be the initiation of the instability. That is, if the deformation is stable, the sheet in region B should be strong enough to provide sufficient supporting force (F_{φ}^{B}) to take the forming force (F_{φ}^{A}) induced by region A, and the deformation is elastic. If not, the sheet in region B reaches its yielding strength, plastic deformation occurs and continues when the tool touches the area down periodically. As a result, the sheet in region B will become thinner and thinner, causing high stress concentration, which leads to the necking and fracture of the sheet finally. Under this situation, the ISF deformation becomes unstable. So the yielding stretching force component is the maximum supporting force region B can provide at one time. This mechanism can be expressed as a normalized form by comparing stretching force from region A and yielding force needed by region B, excluding the effect of parameter K and θ_0 from both sides of equation:

$$\frac{F_{\varphi}^{A}}{K\theta_0} \le \frac{F_{\varphi}^{B}}{K\theta_0} \tag{27}$$

It must be emphasize that this instability criterion can only be applied to ISF process due to its incremental deformation nature and unique tool-sheet contact state. For simpler traditional deformation processes such as pure stretching, Considère's condition may be applied to evaluate the deformation stability directly. However, the underlying logic of these two criteria is the same: when the increasing of the supporting force cannot counterbalance that of the forming force, weak spots appear, which lead to deformation instability.

It can be seen that Eq.27 varies with the material parameter n and the critical forming angle β. However, Eq. 27 is too complex to be solved analytically directly. Instead, by using the MATLAB coding of the equations, the curve of normalized forming force and maximum supporting force can be plotted and compared. As shown in Fig. 3, under a typical forming condition of $r_t = 5mm$, $t_0 = 1mm$, $n=0$, the force variations with different forming angle β can

be obtained. As can be seen in Fig.3, the forming force increases with the increased angle of β . The maximum supporting force increases initially due to the increased area of S. However, after a certain limit, the area S starts to decrease due to the sheet thinning, and the maximum supporting force also decreases. When the forming angle is small, the maximum supporting force is greater than the forming force, thus the deformation is under a stable condition. However, after β increases to a certain level, as the sheet in region B becomes thinner, the maximum supporting force becomes smaller than the forming force, the deformation is no longer stable. As can be seen, the critical condition could be found at the intersection of the two curves. For the given material in this case, the critical condition is reached when the forming angle reaches 79.4° under plane-strain condition and 63.5° under equibiaxial stretching condition.

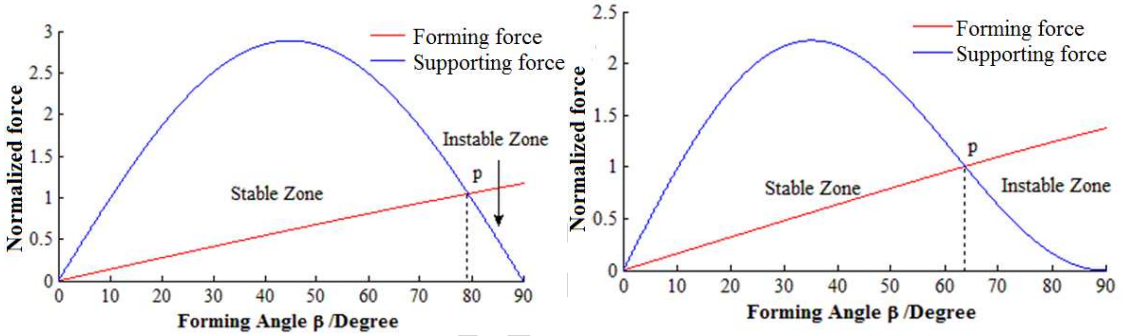

Fig. 3 Comparison of forming force and supporting force: (a) plane-strain condition; (b) equibiaxial stretching condition

The above analysis hypothesizes the deformation stability during ISF process. In the model, the effect of strain hardening is considered by introducing the material hardening exponent *n*. In addition, the ISF sheet deformation is dominated by stretching forming with considerable bending. As shown in Fig. 4, without considering the bending deformation, the stress state becomes pure stretching deformation.

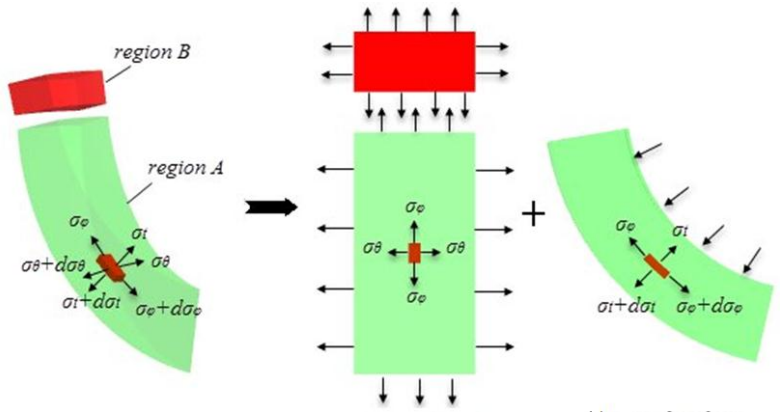

(a) (b) (c)

Fig. 4. Decomposition of ISF stress states: (a) ISF; (b) stretching; (c) bending

Considering the pure stretching without bending, the material in region A yields with increasing stretching force. Under this situation, Negroni and Thomsen [30] employed the Swift law and explained the deformation instability using the following equation:

$$dP_1 = dP_2 = 0 \tag{28}$$

Where P_1 and P_2 are the pulling forces in two in-plane principal directions. Using Eq. 28, the critical strain in the thickness direction was obtained [30].

$$\varepsilon_3 = -\frac{2\cdot(1-\frac{\sigma_2}{\sigma_1}+(\frac{\sigma_2}{\sigma_1})^2)}{4-7\frac{\sigma_2}{\sigma_1}+4(\frac{\sigma_2}{\sigma_1})^2}\cdot n \tag{29}$$

Considering the plane-strain and equibiaxial stretching condition together and neglecting the effect of material anisotropy, the critical strain of deformation instability in the thickness direction can be obtained by using the previously defined parameter m:

$$\varepsilon_3 = -m\cdot n \tag{30}$$

Eq. 30 shows that in the pure stretching, the critical strains are also related to the strain hardening exponent. Using Eq. 27 and 30, the critical strains can be compared between ISF and pure stretching processes.

3. Experimental Validation

To further investigate the ISF deformation stability and fracture mechanism, three experiments, i.e. the universal tensile test, ISF test and bugle test were implemented. As presented in the analytical models, the hardening exponent *n* is a factor affecting deformation

stability. Two materials of Aluminum alloys with varied hardening exponent, AA1100 and AA5052, were tested. For both AA1100 and AA5052, the original sheet thickness is 1.0mm. In all tests, the anisotropic effect was ignored. The flow stress obtained from tensile tests with power law approximation is shown in Fig. 5. As can be seen, due to a low value of hardening exponent, the fracture strain of AA1100 material is only 8%, while that of AA5052 reaches 18%. The material parameters are summarized in Table 1.

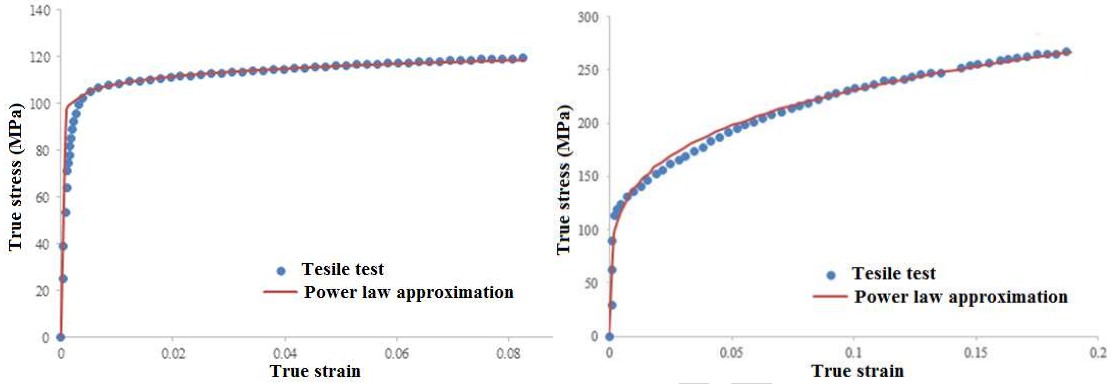

(a) (b)

Fig. 5. Flow stress of materials: (a) AA1100; (b) AA5052

Table 1. Material parameters of AA1100 and AA5052

Material	K	n
AA1100	131.2	0.04
AA5052	388.6	0.23

In the ISF experiments, both cone and pyramid geometries with gradually increased wall angle were produced as shown in Fig. 6. The experiments were conducted on a CNC milling machine with a ball-nose tool of tool radius 5.0mm. During ISF process, the MoS2 powder with grease was used as the lubricant to reduce the friction between the tool and sheet metal. As the forming angle is an effective indicator to evaluate the ISF formability, it was recorded in the experiments. In the experiments, the ISF process would be terminated when the fracture occurred. The fracture height and the corresponding wall angles will be recorded and compared. Fig. 7 shows the finished parts after the ISF experiment. Average fracture height of each part is shown in the respective image of the produced part.

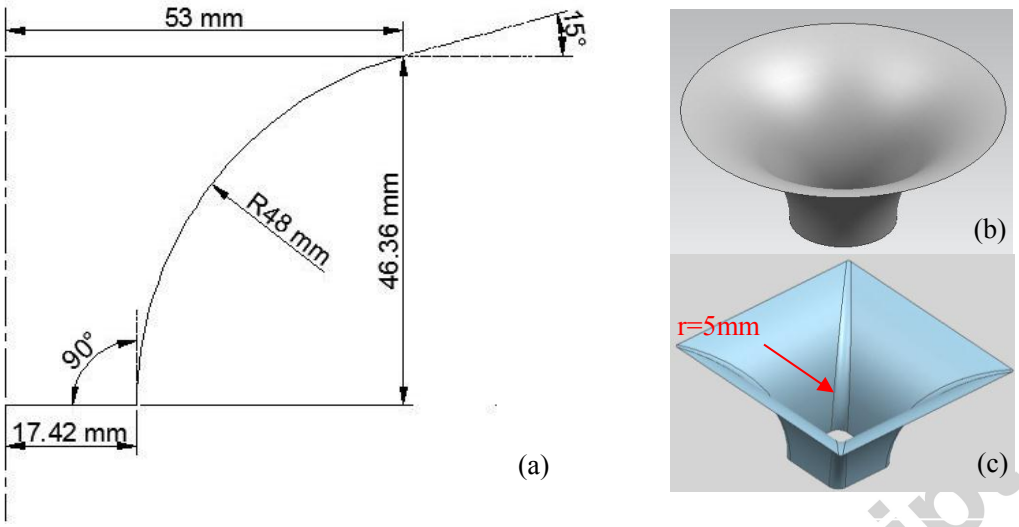

Fig. 6. Geometry of test parts: (a) cross-section of the designed parts; (b) the cone part; (c) the pyramid part

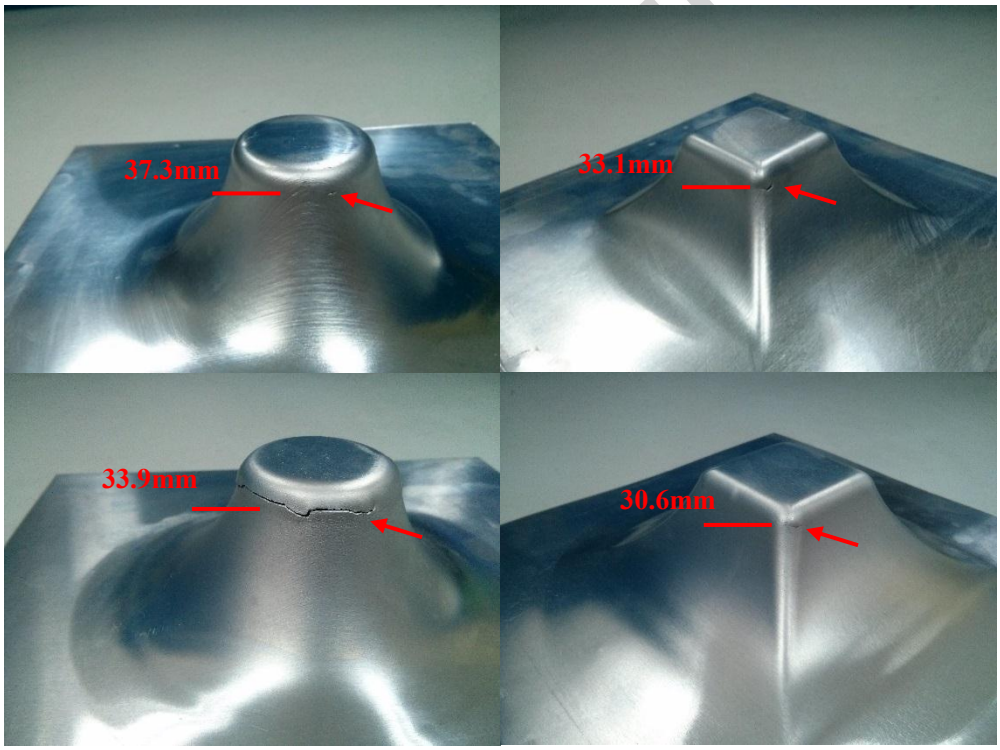

Fig. 7. Macroscopic view of fractured parts: (a) AA1100 cone; (b) AA1100 pyramid; (c) AA5052 cone; (d) AA5052 pyramid

Plane-strain and equibiaxial stretching are the two major deformation modes in the ISF process. The fracture forming limit (FFL) under these two deformation modes was also evaluated by using the bugle test. The tests were performed on BCS-30D general sheet metal

test machine using both AA1100 and AA5052 sheets. Fig. 8 shows the typical specimens of the two materials under the different deformation modes. In the experiment, the GOM digital image correlation (DIC) system was employed and the strain evolutions in the testing process were evaluated.

Fig. 8. Bulge test parts: (a) AA1100 plane-strain; (b) AA5052 plane-strain; (c) AA1100 equibiaxial stretching; (d) AA5052 equibiaxial stretching

4. Analytical and Experimental Results

Using the developed analytical model and the experimental designs, the influence of strain hardening and bending on the deformation stability are investigated. The investigation results are validated by establishing a forming limit diagram (FLD). The predicted forming limit and the experimental results are compared. The observations from FLD are further validated by investigating the fracture behaviour in the experiments.

4.1 Strain hardening effect

Strain hardening plays a significant role in the material plastic deformation in sheet forming process. With the increased strain hardening, the occurrence of necking and deformation instability may be delayed and higher formability can be achieved. Using the developed model, the variation of ISF critical strain expressed as equivalent plastic strain under different deformation states varying with the strain hardening exponent is illustrated in Fig. 9. It can be observed that the critical strain increases with the increasing strain hardening exponent. This is because, with the increase of strain hardening, the deformed material in region B becomes stronger, which could take higher forming force from region A. Concerning the sensitivity of critical strain due to strain hardening, a higher sensitivity can be observed under plane-strain condition than that for the equibiaxial stretching condition. This may be because that under equibiaxial stretching condition, the material yields under the forces from both meridional and circumferential directions, which reduces the sensitivity of critical strain on the force component in the meridional direction.

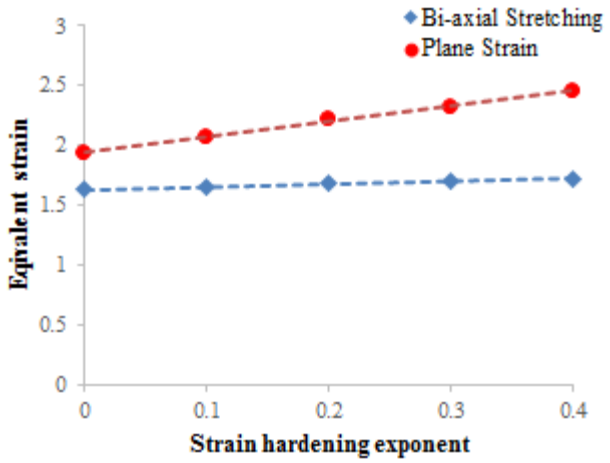

Fig. 9. Influence of strain-hardening coefficient on equivalent strain

4.2 Bending effect

Another significant characterization in the ISF process is the bending deformation of sheet material. In this work, two bending effects are investigated. The first bending effect can be directly obtained from the ISF deformation stability model by using Eq. 30. By keeping the other parameters constant but only changing the ratio of r_t to t_0, the critical strain of deformation instability can be illustrated as shown in Fig. 10. As can be seen, with the increase of bending effect (decrease of r_t/t_0 ratio), the critical strain decreases. This indicates that the bending has a negative effect on the deformation stability. The explanation of this mechanism is straight forward: increasing the bending will introduce a larger tensile stress at the outer surface of the sheet, which increases the forming force. Thus the material in region B will reach the yielding point earlier. This effect can also be validated by the work presented in [11]. In forming the 2A12 sheet, by keeping the tool size the same, increasing the sheet thickness would reduce the ISF forming limit.

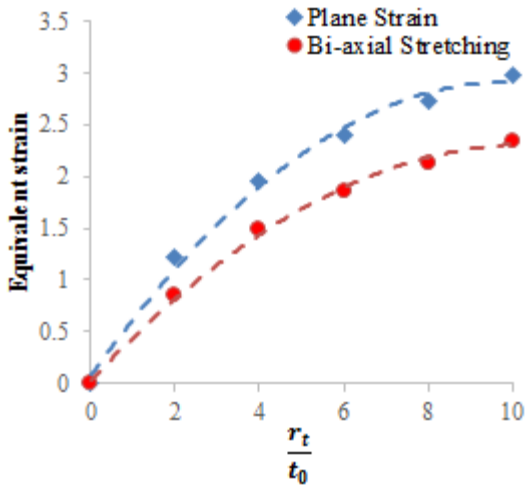

Fig. 10. Influence of bending effect by changing the ratio of tool radius to sheet thickness

Concerning another effect from bending, by comparing the AA1100 tensile test and ISF test results, it can be observed that the material deformation shows obvious differences on the formability in these two processes. In the tensile test, the AA1100 sheet becomes fractured with a strain value of about 0.08 (Fig. 5) while in the ISF test (Fig.7), where the sheet fractures after obvious greater deformation. To explain the fracture strain increase in the ISF process, by employing Eq. 27 and Eq. 30, the critical strain with and without bending effect can be compared with different values of strain hardening exponent as shown in Fig. 11. It is clear that the critical strain obtained from the ISF deformation stability model is much greater than that by using the expanded Swift law. In the pure stretching mode without strain hardening, the material in region B will directly yield as the whole part of region A and B is under the same stress state. However, in the ISF process, due to the sheet bending, the material in region A will start yielding at a lower stretching force. However, this stretching force is not large enough to cause the material yield in region B at the initial forming stage. This is the major cause of the discrepancy of the critical strains between ISF and pure stretching, as can be illustrated in Fig.4.

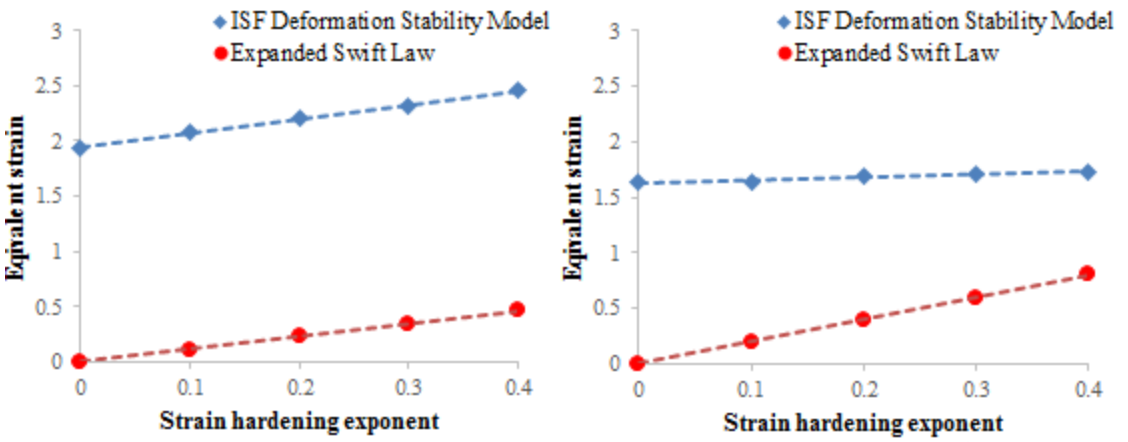

(a) (b)

Fig. 11. Comparison of the ISF and pure stretching deformation stability: (a) plane-strain condition; (b) equibiaxial stretching condition

By analysing the results presented in Fig. 10 and 11, it can be observed that the bending induces two effects: (1) In the ISF process, the bending will generate larger tensile force at the outer surface of the sheet, which causes the earlier sheet fracture. (2) The bending will cause the earlier yielding of the sheet in region A, which could reduce the forming force and increase the deformation stability. By comparing the impacts of these two effects in Fig. 10 and 11, the latter plays a major role.

4.3 Fracture forming limit

The above results are mostly drawn from analytical models. To further investigate the deformation stability and fracture mechanism, an FLD has been produced as shown in Fig. 12. Using the developed model, the predicted ISF critical strains can be plotted in red lines as shown in Fig. 12. In addition, the fracture forming limit (FFL) obtained from bugle test, as an indication of formability associated with the material property, is plotted by using black lines. These forming limits are compared with the actual fracture strain obtained from ISF experiments. As can be seen, for the AA1100 material, the fracture occurs in the ISF process before reach the FFL. The actual fracture in the ISF test is more close to the prediction results. However, the AA5052 sheet shows a different relationship. The predicted critical strain is much higher, while the FFL is much lower. The actual fracture of AA5052 in the ISF experiment is more close to the FFL. This result suggests that the ISF formability does not obey a generalized rule but depends on the relationships between FFL and deformation stability. For some materials, the deformation instability is the dominate effect that causes the

sheet fracture while for other materials, the facture occurs because the deformation reaches the FFL first. When either the FFL or the ISF deformation instability conditions can be satisfied, the sheet crack will occur.

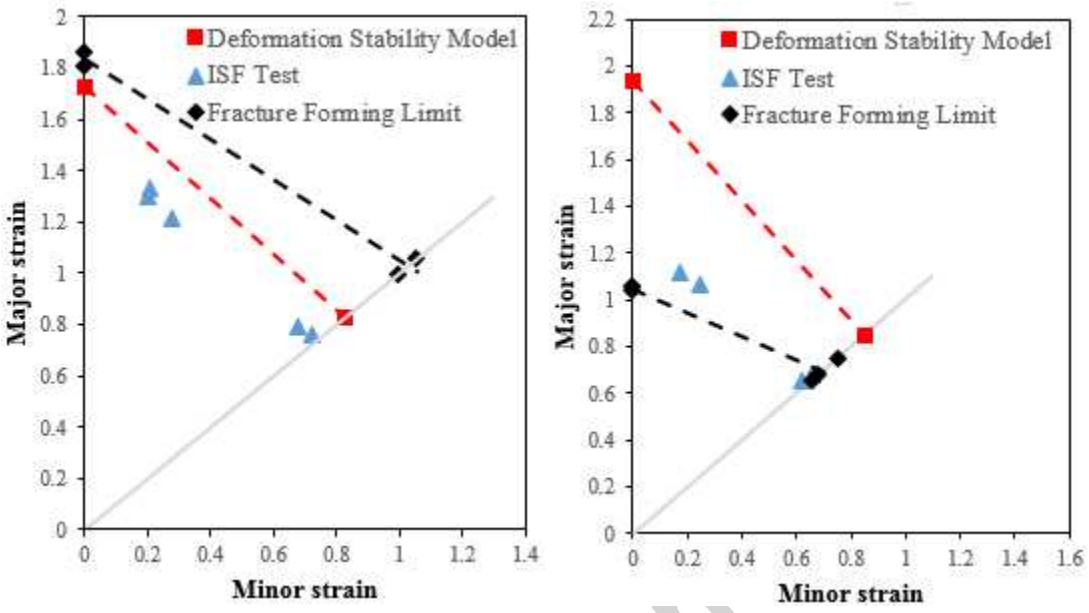

(a) (b)

Fig. 12. Comparison of formability: (a) AA1100; (b) AA5052

4.4 Fracture behavior

The results presented in Fig.12 suggest that the AA1100 and AA5052 show different fracture characterizations: the AA1100 parts cracked due to the loss of deformation stability while for the AA5052 part, the fracture occurs because it reaches the FFL. To further confirm this hypothesis, the ISF parts are examined by investigating the cross-sectional profile at the fracture location.

As shown in Fig. 13, for the AA1100 parts, obvious necking can be observed in both ISF and bugle tests. In the ISF test as shown in Fig. 13(a) & (b), in both cases of plane-strain and equibiaxial stretching conditions, when the sheet thickness reaches about 0.22mm or 0.21mm respectively, the necking starts developing. However, in the bugle test as shown in Fig. 13(c) & (d), the necking started at an earlier stage, about 0.77mm in thickness under plane-strain condition and 0.57mm in thickness under equibiaxial stretching condition. Concerning the fracture thickness, under both plane-strain and equibiaxial stretching condition, the similar thickness was observed between ISF and bulge tests respectively. This observation suggests that although the sheet starts necking at different forming stage, the final fracture thickness is similar. The ISF process could delay the occurrence of necking but the deformation instability

occurs before reaching the material fracture limit.

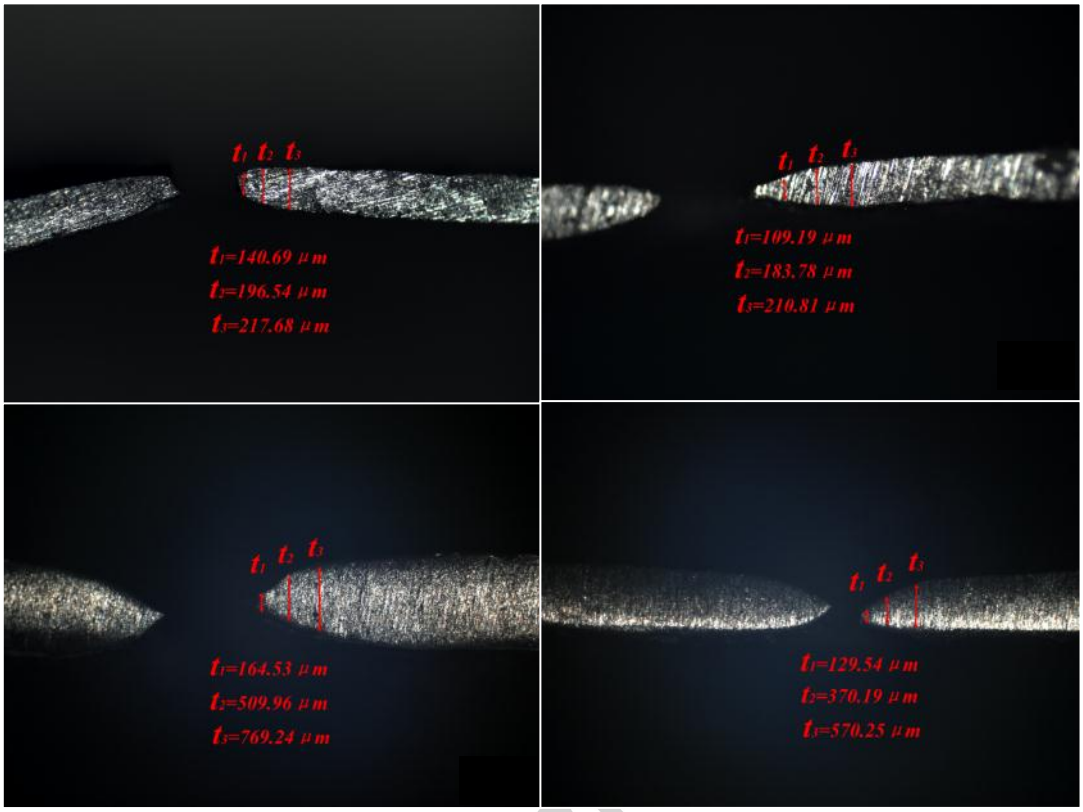

Fig. 13. Cross-sectional view of the fracture region for AA1100 material: (a) cone part in ISF test; (b) pyramid part in ISF test; (c) bulge test part under plane-strain condition; (d) bulge test part under equibiaxial stretching condition

For the AA5052 sheets, no obvious necking can be observed in the ISF test as shown in Fig. 14(a) & (b). The thickness at the fracture location is about 0.35mm under plane-strain condition and about 0.26mm under equibiaxial stretching condition. As there is no obvious reduction in thickness, the sheet fracture occurs immediately when the deformation reaches the FFL. Concerning the facture behavior in the bugle test, obvious necking can be observed. However, comparing the fracture thickness between ISF and bugle test, the sheet fracture thickness is similar under plane-strain and equibiaxial stretching condition respectively. This result shows that there is no sign of the occurrence of deformation instability in the ISF process for AA5052. The sheet fractures because it reaches its FFL.

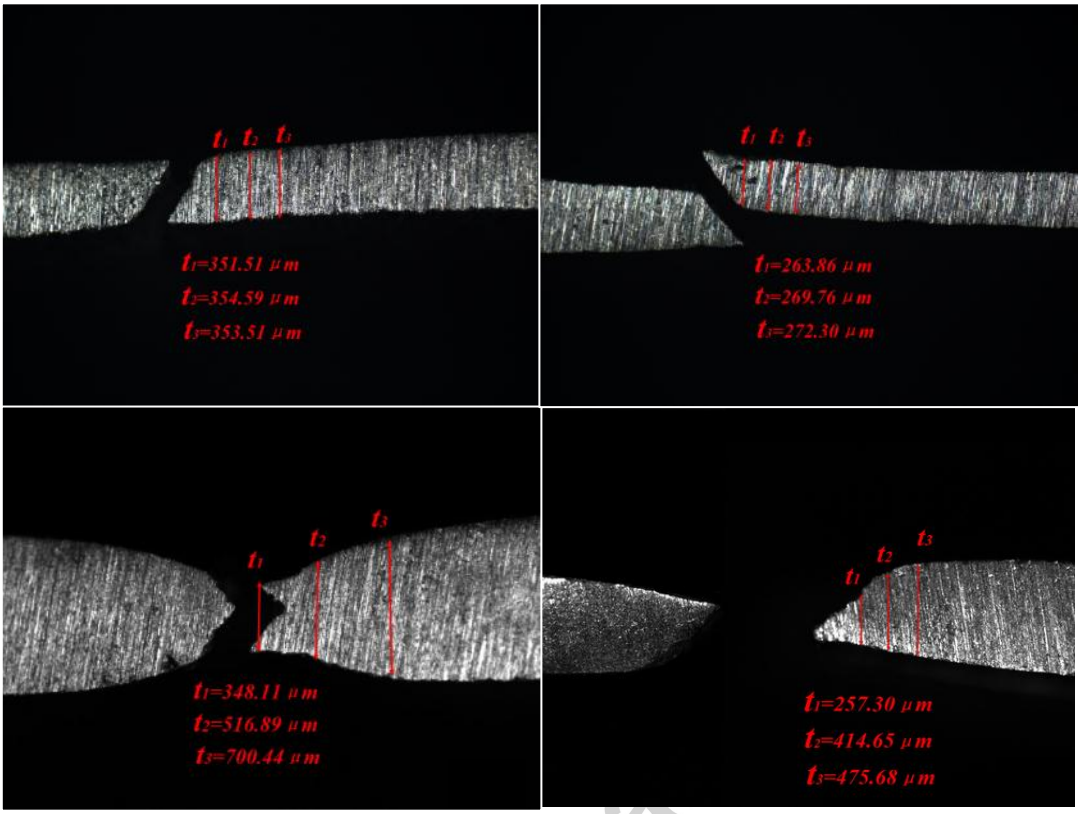

Fig. 14. Cross-sectional view of the fracture along meridional direction for AA5052 material: (a) cone part; (b) pyramid part in ISF test; (c) bulge test part under plane-strain condition; (d) bulge test part under equibiaxial stretching condition

The results in Fig. 13 and 14 could confirm the hypothesis that the ISF formability does not obey a generalized rule: if the deformation instability condition reaches first, the fracture occurs due to deformation instability; if the material FFL reaches first, the fracture occurs due to the limited ductility of the material itself.

4.5 Discussions of results

By summarizing the analytical and experimental results obtained in this study, it can be concluded that there are two major fracture mechanisms in ISF process: 1) fracture due to limited material ductility and 2) fracture due to the loss of deformation stability. When the sheet deformation shifts from stretching deformation to a combined stretching and bending in ISF, the material ductility is kept unchanged. The increased ISF formability majorly comes from the enhancement of deformation stability. A good example is the deformation of AA1100 material: the strain at fracture in the universal tensile test is only 0.08 while that in ISF is over

1.00. However, for the AA5052 material, this increase is less obvious due to the limited material ductility.

Concerning the strain hardening effect, as observed in Fig. 9, the strain hardening has a positive effect on the deformation stability. An increase of 0.1 in hardening exponent would increase the critical strain by 0.16 under plane-strain condition and 0.06 under equibiaxial stretching condition. Fig. 11 suggests that the sensitivity of the critical strain on the hardening exponent is similar in both ISF and pure stretching. However, although the strain hardening plays a similar role in the two processes, it becomes less obvious in ISF as this effect is overshadowed by the bending effect.

Concerning the bending effect, although a larger bending deformation could increase the tensile stress at the outer surface of the sheet, it is also a major factor to enhance the ISF deformation stability. This work has analytically proven and experimentally validated this hypothesis. The increased ISF formability is achieved through the enhanced deformation stability: comparing to pure stretching, bending would cause the material yields at a lower forming force. Under this situation, the region B could support the stretching force from region A without failure. However, the increased formability in ISF will be more obvious in forming the sheet material with low strain hardening but high ductility. For the sheet metal with limited ductility, the formability cannot be improved much in single point incremental forming. Alternative approaches such as the double side incremental forming or hot ISF methods maybe a better solution via improving the stress triaxiality or increasing the forming temperature.

5. Conclusions

In this study, the deformation stability and the fracture mechanism in the ISF process have been studied. Two key factors that affecting the deformation stability, including strain hardening and bending, have been investigated based on a developed analytical model and a series of experiments. From this work, the following conclusions may be drawn:

(1) Sheet fracture in the ISF process could either be caused by the deformation instability or limited material ductility. Sheet fracture occurs when either of the failure limits is reached.

(2) Bending is a major cause of the enhanced ISF formability: the sheet in region A could yield with a lower forming force, which delays the occurrence of the deformation instability in region B.

(3) Strain hardening plays the same role in ISF and stretching. However, this effect is less obvious in ISF as it is overshadowed by the bending effect.

(4) The enhancement of ISF formability is more obvious in processing material with lower strain hardening exponent but higher ductility. For material with limited ductility, the improvement of ISF formability is limited.

Acknowledgement

The authors are grateful for the financial support from the National Key Specific Science & Technology Program from Ministry of Industry and Information Technology of China through Grant # 2011ZX04016-051 and financial support from National Natural Science Foundation of China through Grant #51675332, and the support provided by the Marie Curie International Incoming Fellowship (628055 & 913055) and International Research Staff Exchange Scheme (IRSES, MatProFuture project, 318968) within the 7th EC Framework Programme (FP7).

References

[1] S. Matsubara, Incremental Backward Bulge Forming of a Sheet Metal with a Hemispherical Head Tool-A Study of a Numerical Control Forming System II, Journal-Japan Society For Technology Of Plasticity, 35 (1994) 1311-1311.
[2] R. Malhotra, J. Cao, M. Beltran, D. Xu, J. Magargee, V. Kiridena, Z.C. Xia, Accumulative-DSIF strategy for enhancing process capabilities in incremental forming, CIRP Annals-Manufacturing Technology, 61 (2012) 251-254.
[3] J. Duflou, B. Callebaut, J. Verbert, H. De Baerdemaeker, Laser assisted incremental forming: formability and accuracy improvement, CIRP Annals-Manufacturing Technology, 56 (2007) 273-276.
[4] G. Fan, L. Gao, G. Hussain, Z. Wu, Electric hot incremental forming: a novel technique, International Journal of Machine Tools and Manufacture, 48 (2008) 1688-1692.
[5] M. Silva, M. Skjødt, P.A. Martins, N. Bay, Revisiting the fundamentals of single point incremental forming by means of membrane analysis, International Journal of Machine Tools and Manufacture, 48 (2008) 73-83.
[6] P. Martins, N. Bay, M. Skjødt, M. Silva, Theory of single point incremental forming, CIRP Annals-Manufacturing Technology, 57 (2008) 247-252.
[7] D. Xu, W. Wu, R. Malhotra, J. Chen, B. Lu, J. Cao, Mechanism investigation for the influence of tool rotation and laser surface texturing (LST) on formability in single point incremental forming, International Journal of Machine Tools and Manufacture, 73 (2013) 37-46.
[8] L. Fratini, G. Ambrogio, R. Di Lorenzo, L. Filice, F. Micari, Influence of mechanical properties of the sheet material on formability in single point incremental forming, CIRP Annals-Manufacturing Technology, 53 (2004) 207-210.
[9] B. Lu, J. Chen, H. Ou, J. Cao, Feature-based tool path generation approach for incremental sheet forming process, Journal of Materials Processing Technology, 213 (2013) 1221-1233.
[10] Y. Kim, J. Park, Effect of process parameters on formability in incremental forming of sheet metal, Journal of materials processing technology, 130 (2002) 42-46.
[11] Y. Fang, B. Lu, J. Chen, D. Xu, H. Ou, Analytical and experimental investigations on deformation mechanism and fracture behavior in single point incremental forming, Journal of Materials Processing Technology, 214 (2014) 1503-1515.
[12] B. Lu, Y. Fang, D. Xu, J. Chen, H. Ou, N. Moser, J. Cao, Mechanism investigation of friction-related effects in single point incremental forming using a developed oblique roller-ball tool, International Journal of Machine Tools and Manufacture, 85 (2014) 14-29.
[13] Y. Huang, J. Cao, S. Smith, B. Woody, J. Ziegert, M. Li, Studies of size effect on the formability of a domed part in incremental forming, Proceedings of the 2008 International Manufacturing Science and

Engineering Conference, Illinois, USA, 2008.
[14] M.-S. Shim, J.-J. Park, The formability of aluminum sheet in incremental forming, Journal of Materials Processing Technology, 113 (2001) 654-658.
[15] J.-J. Park, Y.-H. Kim, Fundamental studies on the incremental sheet metal forming technique, Journal of Materials Processing Technology, 140 (2003) 447-453.
[16] D. Young, J. Jeswiet, Wall thickness variations in single-point incremental forming, Proceedings of the Institution of Mechanical Engineers, Part B: Journal of Engineering Manufacture, 218 (2004) 1453-1459.
[17] T. Kim, D. Yang, Improvement of formability for the incremental sheet metal forming process, International Journal of Mechanical Sciences, 42 (2000) 1271-1286.
[18] L. Filice, L. Fratini, F. Micari, Analysis of material formability in incremental forming, CIRP annals-Manufacturing technology, 51 (2002) 199-202.
[19] W. Emmens, A. Van den Boogaard, Incremental forming by continuous bending under tension—an experimental investigation, Journal of Materials Processing Technology, 209 (2009) 5456-5463.
[20] K. Jackson, J. Allwood, The mechanics of incremental sheet forming, Journal of materials processing technology, 209 (2009) 1158-1174.
[21] J.M. Allwood, D.R. Shouler, Generalised forming limit diagrams showing increased forming limits with non-planar stress states, International Journal of Plasticity, 25 (2009) 1207-1230.
[22] P. Eyckens, A. Van Bael, P. Van Houtte, Marciniak–Kuczynski type modelling of the effect of through-thickness shear on the forming limits of sheet metal, International Journal of Plasticity, 25 (2009) 2249-2268.
[23] R. Malhotra, L. Xue, T. Belytschko, J. Cao, Mechanics of fracture in single point incremental forming, Journal of Materials Processing Technology, 212 (2012) 1573-1590.
[24] W. Emmens, A. Van den Boogaard, An overview of stabilizing deformation mechanisms in incremental sheet forming, Journal of Materials Processing Technology, 209 (2009) 3688-3695.
[25] P. Eyckens, B. Belkassem, C. Henrard, J. Gu, H. Sol, A.M. Habraken, J.R. Duflou, A. Van Bael, P. Van Houtte, Strain evolution in the single point incremental forming process: digital image correlation measurement and finite element prediction, International journal of material forming, 4 (2011) 55-71.
[26] M.B. Silva, P.S. Nielsen, N. Bay, P. Martins, Failure mechanisms in single-point incremental forming of metals, The International Journal of Advanced Manufacturing Technology, 56 (2011) 893-903.
[27] Lu, B., et al. "Investigation of material deformation mechanism in double side incremental sheet forming." International Journal of Machine Tools and Manufacture 93 (2015): 37-48.
[28] Jackson, K. P., J. M. Allwood, and M. Landert. "Incremental forming of sandwich panels." Journal of Materials Processing Technology 204.1 (2008): 290-303.
[29] Allwood, J. M., D. R. Shouler, and A. E. Tekkaya. "The increased forming limits of incremental sheet forming processes." Key Engineering Materials344 (2007): 621-628.
[30] F. Negroni, S. Kobayashi, E.G. Thomsen, Plastic instability in simple stretching of sheet metals, Journal of Manufacturing Science and Engineering, 90 (1968) 387-392.

Highlights

- A new model is proposed to analyze the deformation stability in single point incremental sheet forming based on the previous experimental observation.
- Two deformation modes, plane strain and equibixial tension, are both considered in the model.
- By comparing the shapes of the cracks and the theoretical model, a comprehensive failure mechanism for ISF is proposed. Sheet metal can fail because of the excessive stretching stress or the limitation of their own formability.